



Research Article

Ni and Mn enrichment effects on reformed austenite: thermodynamical and low cycle fatigue stability of 13%Cr–4%Ni and 13%Cr–6%Ni stainless steels

Stéphane Godin¹  · Johann Hamel-Akré² · Denis Thibault¹ · Alessandra-Maria Serventi¹ · Philippe Bocher²

Received: 5 November 2019 / Accepted: 4 February 2020 / Published online: 11 February 2020
© Springer Nature Switzerland AG 2020

Abstract

By comparing the behavior of 13%Cr–4Ni and 13%Cr–6Ni alloys, this paper investigated the effect of Ni and Mn enrichment on the amount, mechanical stability, and microstructure of reformed austenite. 4%Ni and 6%Ni–1.5%Mn weld multilayer deposits were made and heat treated to stabilize various amounts of austenite content at room temperature. The maximum austenite content has been obtained at the same temperature (630 °C for 1 h) for both alloys, but 3.6 times more austenite content was formed in the 6%Ni steel. For both alloys similar austenite contents were obtained by post-weld heat treating at different temperatures and were compared experimentally. Results showed that with the addition of Ni and Mn, thinner and lower Ni content austenite was formed. Moreover, austenite generated at lower temperature was mechanically more stable under low cycle fatigue loading. Its rate of transformation has been reduced by a factor of 2.3, resulting in the stabilization of twice more austenite after 20 cycles at 2% strain considering the results of the present study, it is concluded that Ni and Mn contents do significantly affect the mechanical stability of reformed austenite; furthermore austenite lamellae morphology and thickness also seem to play a significant role in stabilizing this phase.

Keywords Reformed austenite · Mechanical stability · Martensite · Stainless steel

1 Introduction

Soft martensitic stainless steels 13%Cr–4%Ni steels (ASTM A240 and ASTM A743) are used for the manufacturing hydraulic turbine runners. These materials offer good mechanical properties, good cavitation erosion resistance and good toughness [1–3]. They are called “soft martensitic” because they contain less than 0.06% carbon [4, 5], allowing them to be easily assembled by FCAW or GMAW welding processes. The filler materials normally used for welding is ER410NiMo that contains up to 4% nickel.

In the as-cast, hot-rolled, or as-welded conditions, soft martensitic stainless steels are mainly composed of

martensite, delta ferrite (up to 10%), retained austenite and carbides [1, 3, 6]. However, heated above 550 °C, a certain amount of martensite transforms to austenite (this austenite is called reverted austenite) and can be stabilized upon cooling down to room temperature due to its enrichment in austenite stabilizing elements. The reverted austenite stable at low temperatures is called reformed austenite forming a dispersion of austenite precipitates or austenite lamellae that remains stable upon quenching at temperatures as low as –196 °C [1]. Higher tempering temperatures result in higher reverted austenite percentages; however, if the tempering temperature is too high within the intercritical phase field, austenite stabilizers

✉ Stéphane Godin, godin.stephane@ireq.ca; Johann Hamel-Akré, johann.akre@gmail.com; Denis Thibault, thibault.denis@ireq.ca; Alessandra-Maria Serventi, serventi.alessandra-maria@ireq.ca; Philippe Bocher, philippe.bocher@etsmtl.ca | ¹Institut de Recherche d’Hydro-Québec, 1800 boul. Lionel Boulet, Varennes, QC J3X 1S1, Canada. ²École de technologie supérieure, 1100 rue Notre-Dame Ouest, Montréal, QC H3C 1K3, Canada.



elements Ni and Mn will be diluted into a higher fraction of reverted austenite and transform back to a hard and brittle “fresh” martensite upon cooling to room temperature [7, 8]. Depending on steel compositions and how heat treatments are optimized, 25% of reformed austenite stable at room temperature can be obtained when a double tempering treatment is used in 4%Ni steels, and percentage as high as 40% in 6%Ni steel can be reached even for a single stage tempering [9, 10].

Despite the fact that reformed austenite is stable in its tempered martensite matrix, martensitic transformation can occur in the reformed austenite when mechanical work is applied to the steel [11]. The transformation of mechanically unstable austenite is well known to be responsible for transformation induced plasticity (TRIP effect). The TRIP effect provides excellent mechanical properties to the steel and has been used to design so-called TRIP steels containing residual austenite (in this case, the austenite remains stable due to some specific cooling conditions that prevent its full transformation to martensite, bainite, or ferrite). The residual and reformed austenite can also transform in the context of low cycle fatigue tests (LCF) or fatigue crack-propagation. This has been studied in steels by various authors [12, 13], but only few studies are available for low-carbon soft martensitic stainless steels [14, 15].

A previous study focusing on the mechanical stability under low cycle fatigue (LCF) of reformed austenite in UNS S41500 steel has shown that the amount of reformed austenite rapidly decreases with the number of cycles to reach an asymptotic value that does not transform even when fracture occurs [16]. These LCF results have shown that the sample containing the highest austenite amount undergoes a higher rate of TRIP transformation; this suggests that a higher fraction of austenite tends to reduce the stability of the phase to transformation during mechanical testing. Unfortunately, as this work did not document the austenite chemical compositions, it was not possible to fully assess the origin of reformed austenite stability. Such measurements were done later in another study for a 13%Cr–4%Ni steel [16], suggesting that Ni content in austenite may be the main factor driving for the formation of reformed austenite and the austenite stability. The

correlation between austenite chemical composition and its overall mechanical stability can however not be made trivially: transformation can occur under mechanical stress or can be induced by strain. Moreover, besides austenite stabilizers content other parameters can play a significant role, such as particles volume and size, matrix hardness, etc. [17].

Following these findings, the focus of the present study is to provide more data on the role of austenite stabilizers such as Ni on the LCF austenite mechanical stability in soft martensitic stainless steels. In the present work, multi-layer deposits made of 13%Cr–4%Ni steel and 13%Cr–6%Ni steel were made. Since Mn content was also different in both fillers—Mn is also known to be an austenite stabilizer and to decrease M_s temperature in steels [18, 19]—this element was taken into consideration. Thus, the effects of Ni and Mn on the microstructure and amount of reformed austenite were studied as a function of the tempering conditions. The mechanical stability of the reformed austenite in these alloys was documented for LCF tests at 2% strain; both steels were compared at equivalent amount of reformed austenite (8%) and at their maximum percentage of reformed austenite. Thermo-Calc Software TCFE7 Steels/Fe-alloys database version 7 was used to estimate the equilibrium austenite composition at the tempering temperatures [20, 21]. The results were then compared with the experimental data in order to provide a physical basis to explain the mechanical behavior of the reformed austenite.

2 Experimental procedure

2-cm thick multi-layer deposits were made on UNS S41500 stainless steel plates of 15.2 cm × 30.4 cm × 5.6 cm using a robot. A commercial 13%Cr–4%Ni–0.4%Mn filler alloy was used as reference and a proprietary 13%Cr–6%Ni–1.6%Mn experimental filler alloy was used to study the effect of Ni and Mn enrichment. Welding parameters are presented in Table 1.

The actual chemical composition of the plates and the weld deposits were measured using standards ASTM E1019 and ASTM E1479 methods. Carbon, sulfur, oxygen,

Table 1 Welding parameters

| Filler | Process | Gas | Preheat temp. (°C) | Interpass temp. (°C) | Current (A) | Voltage (V) | Speed (mm/s) | Heat input (kJ/mm) |
|------------|---------|------------------------|--------------------|----------------------|-------------|-------------|--------------|--------------------|
| 13%Cr–4%Ni | FCAW | 75Ar–25CO ₂ | 100 | 160 | 333 | 31 | 8 | 1.3 |
| 13%Cr–6%Ni | MCAW | 92Ar–8CO ₂ | 100 | 125 | 277 | 28 | 6.6 | 1.2 |

FCAW flux core arc welding, MCAW metal core arc welding

and nitrogen contents were measured by Combustion and Inert Gas Fuel (ASTM E1019), the other elements by Inductively-Coupled Plasma Atomic Emission Spectrometer (ASTM E1479). One sample of each was measured. Chemical compositions of base metal and welding deposits are presented in Table 2.

In order to define the temperatures at which martensite starts to transform to austenite under heating (A_{C1}) and at which transformation to austenite is completed, dilatometry analyses were realized for both deposits after welding. Samples of 3 mm × 3 mm × 10 mm were machined and put into a *TMA Q400* tester from 23–850 °C to 850–23 °C at a 2 °C/min rate without any holding time. Curves were plotted to measure and compare A_{C1} , A_{C3} and M_s for both deposits. These temperatures were then used to choose the tempering temperatures for experiment design.

Figure 1 provides a visual comparison of the A_{C1} , A_{C3} , and M_s of both deposits. 13%Cr–6%Ni steel curve is shifted down to lower temperatures compared to the 4%Ni steel curve, confirming that its A_{C1} , A_{C3} and M_s temperatures were lower. The curves show that austenite reversion begins at 597 °C for the 13%Cr–4%Ni steel and 547 °C for 13%Cr–6%Ni steel. The transformation is completed at 798 °C and 710 °C, respectively. The M_s values were found to be respectively 284 °C and 187 °C. These lower values found in 13%Cr–6%Ni steel can be attributed to the higher elements content of the alloy.

After welding, both welds were austenitised at 1100 °C for 2 h to both homogenize the deposit microstructures and to minimise the effect of multipass welding. One hour temper treatments were done in a *Carbolite* recirculating furnace at temperatures ranging from 430 to 690 °C to generate various amounts of reformed austenite. The volume fraction of the resulting phases was quantified by X-ray diffraction (XRD) analysis after tempering, with a *Bruker D8 Advance diffractometer* using Cu K α radiation. XRD patterns were collected in the range $40^\circ \leq 2\theta \leq 140^\circ$ with a 0.05° resolution. Rietveld analysis was performed to quantify the reformed austenite using *Topas* software. The absolute error on the measurement was estimated around $\pm 1.5\%$. Rockwell C hardness (150 kg load with a conical diamond as penetrator) was then performed on each deposit for comparison. Five indents per sample were realized using a *Zwick ZHU250* universal hardness tester.

In order to analyze the effect of tempering on the microstructure, material investigations were carried out

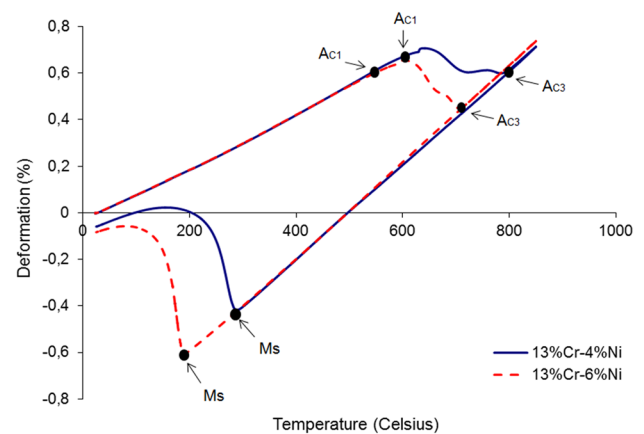


Fig. 1 Dilatometry curves of the 13%Cr–4%Ni and 13%Cr–6%Ni steels showing temperatures A_{C1} , A_{C3} , and M_s at 2 °C/min rate

by scanning and transmission electron microscopy. The scanning electron microscope (SEM) S-4700 was operated at the acceleration voltage of 5 kV. Moreover, the Hitachi H-9000 transmission electron microscope was used at the acceleration voltage of 300 kV to realize bright and dark field observations of samples. Microstructure images were presented with their corresponding selected area electron diffraction (SAED) patterns to identify the presence of austenite phase inside the martensitic matrix. In this work, a scanning transmission electron microscopy Hitachi STEM HD-2700 was also used at the high voltage of 200 kV. This instrument is equipped with EDX spectrometer (energy dispersive X-ray spectroscopy) necessary to realize chemical microanalysis of materials.

To realize such electron microscopy observations, materials have to be submitted to a specific preparation procedure. Samples for SEM observation were electropolished with a *Lectropol-5* unit from *Struers* using perchloric acid as electrolyte. STEM and TEM thin films were prepared by using Focused Ion Beam (FIB) with a *Hitachi nanoduet NB5000* instrument.

Thermo-Calc Software was used to predict the chemical thermodynamics of reverted austenite. Thermo-Calc Software TCFE7 Steels/Fe-alloys database version 7 has been used to predict the equilibrium austenite enrichment in solutes chromium, manganese, nickel and carbon that can be compared to measured values. In addition, Thermo-Calc Software models can predict the composition and

Table 2 Chemical composition of base metal and deposits (wt% and *mass ppm)

| Steels | C | Cr | Ni | Mn | Mo | Si | Cu | S* | P* | O* | N* |
|------------|-------|------|------|------|------|------|------|----|-----|-----|-----|
| UNS S41500 | 0.030 | 12.5 | 3.78 | 0.68 | 0.59 | 0.41 | 0.08 | 10 | 130 | 50 | 310 |
| 13%Cr–4%Ni | 0.018 | 12.6 | 4.62 | 0.39 | 0.61 | 0.43 | 0.05 | 90 | 70 | 450 | 200 |
| 13%Cr–6%Ni | 0.012 | 13.1 | 6.24 | 1.46 | 0.06 | 0.72 | 0.01 | 80 | 70 | 330 | 290 |

maximum amount of reverted austenite to be formed at equilibrium in both alloys at temperatures above the intercritical temperature for austenite reversion. From these results and assuming ortho-equilibrium conditions, Ghosh and Olson method [22, 23] was used to rely the energy required for partial dislocation networks surrounding martensitic nuclei to propagate into austenite and estimate M_s values for a given microstructure. Assuming that martensitic transformation can take place from tiny pre-existing embryos having martensitic structures growing in the austenite, they have described this transformation using a dislocation model that can predict the interfacial stress field, the energy, the stability and interfacial mobility of the defect. M_s becomes the temperature at which the embryos, treated as dislocations, can propagate freely. Interestingly, Ghosh and Olson also ruled out the role of Peierls barrier on the motion of martensitic interface during transformation in materials with metallic bonding, following Grujicic et al. [24].

Finally, the mechanical stability of this reformed austenite was studied at room temperature using LCF tests according to ASTM E606-04 standard. Tests were conducted on samples containing the maximum possible amounts of austenite in both steels and also on samples containing a fixed volume fraction of 8%. The round samples were polished from 1200 SiC grits to 1 μm diamond paste to get a mirror finish with a roughness lower than 0.2 Ra. LCF tests were made on a 100 kN servo hydraulic *Instron* tester. *Wood's* metal system alignment was used as grip fixtures. An *Instron 2620-827* extensometer was chosen to control the deformation applied to the samples. The tests were realized at 23 $^{\circ}\text{C}$, under a strain amplitude of 2% and a strain ratio of $R = -1$ (sine waveform of 0.1 Hz).

3 Sample design and LCF results

Austenite percentages measured after 1 h intercritical tempering are plotted against time in the graph of Fig. 2. A "bell shaped" curve was found for both steels, however the curve is shifted to lower temperatures for 13%Cr–6%Ni steel, reaching significantly higher reformed austenite amount. More specifically, in 13%Cr–4%Ni steel austenite reversion starts at 550 $^{\circ}\text{C}$ (A_{C1} temperature) and is stabilized up to a maximum of 8% at 630 $^{\circ}\text{C}$. In the 13%Cr–6%Ni steel, reverted austenite can be found after tempering as low as 510 $^{\circ}\text{C}$ and its maximum content is found at the same temperature as 13%Cr–4%Ni steel. However, the maximum fraction is 3.6 times larger i.e. up to 29%. When tempering above the temperature of maximum content, the reformed austenite content gradually decreases with tempering temperature, and vanishes if tempered around 690 $^{\circ}\text{C}$ for both alloys. So, higher content of Ni and Mn

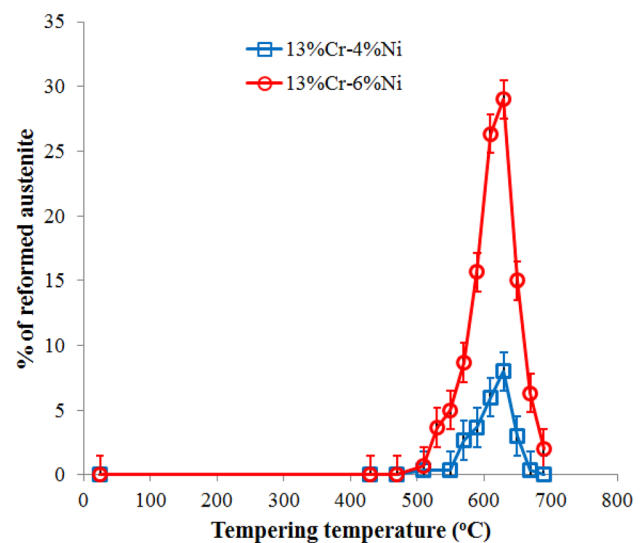


Fig. 2 Reformed austenite percentage versus tempering temperature (1 h) for 13%Cr–4%Ni and 13%Cr–6%Ni deposits. Error bars represent the absolute error on the measurements

Table 3 A_{C1} from TMA and XRD analysis

| Steels | A_{C1} (TMA) (2 $^{\circ}\text{C}/\text{min}$) ($^{\circ}\text{C}$) | A_{C1} (XRD) (1 h tempering) ($^{\circ}\text{C}$) |
|------------|--|---|
| 13%Cr–4%Ni | 597 | 550 |
| 13%Cr–6%Ni | 547 | 510 |

in 13%Cr–6%Ni have extended its temperature range for austenite reversion to lower temperatures and increased the maximum amount of reverted austenite stable at room temperature.

It is interesting to compare the A_{C1} values obtained by dilatometry to the isothermally transformed samples. The values obtained from the 1 h tempering treatments are significantly lower than the values measured by dilatometry analysis (see Table 3), illustrating that diffusion process play a significant role in the nucleation and early growth of the phase. Isothermal treatments gives ample time for austenite germs to reach large enough sizes (to incubate) and grow past the nucleation barrier.

Regarding hardness measurements versus tempering temperatures, it can be seen that for both alloys the hardness decreases from A_{C1} to 630 $^{\circ}\text{C}$ and increases to A_{C3} (see Fig. 3). This hardness decrease is mainly associated with the increase in reformed austenite content and with the tempering of martensite [16, 25]. On the other hand, hardness increase in the range 630 $^{\circ}\text{C}$ to A_{C3} can be attributed to the transformation of part of the reverted austenite to fresh martensite upon cooling. The fresh

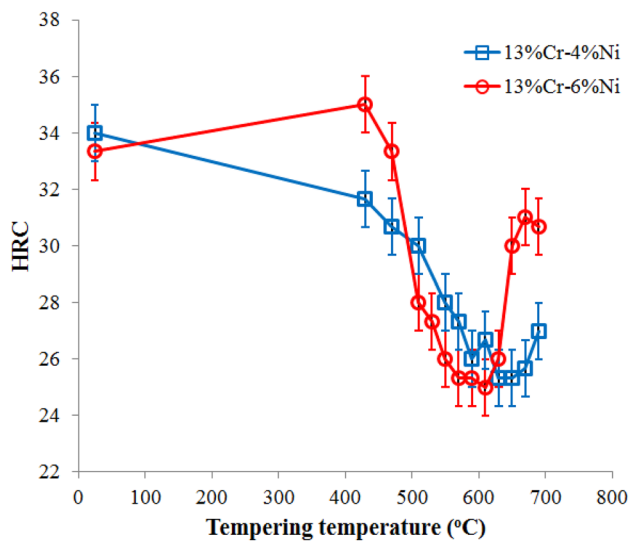


Fig. 3 Hardness versus tempering temperature (1 h) for 13%Cr-4%Ni and 13%Cr-6%Ni deposits. Error bars represent the absolute error on the measurements

martensite formed from reverted austenite is harder than the tempered martensite due to the presence of numerous dislocation tangles resulting from the transformation and slightly higher carbon content. Minimal hardness for both steels corresponds to the maximum content of reverted austenite stabilized at room temperature.

Some hardness differences between the two alloys were observed. The higher content of alloying elements in the 13%Cr-6%Ni steel (21.7 wt% against 18.8 wt%), could result in a higher hardness due to solid solution hardening; however the as-welded was found to be less hard than the 13%Cr-4%Ni steel. The higher carbon content of the 13%Cr-4%Ni steel (0.018% vs. 0.012% as seen in Table 2) and different cooling rates due to different welding parameters could explain this difference in initial hardness. When tempered at 430 °C, the 13%Cr-4%Ni steel sees its hardness drop whereas the 13%Cr-6%Ni steel displays a significant increase in hardness. This suggests that precipitation hardening may take place in this alloy, compensating for martensite softening induced by tempering. The hardness behavior for both alloys are similar in the range 510–630 °C, with a lower hardness by about 2 HRC for the 13%Cr-6%Ni steel, most likely due to its higher austenite content.

3.1 Austenite stability under LCF tests

Based on the above results, three samples have been chosen for mechanical testing to compare the relative stability of their reformed austenite: one sample of reference from 13%Cr-4%Ni steel have been chosen, and

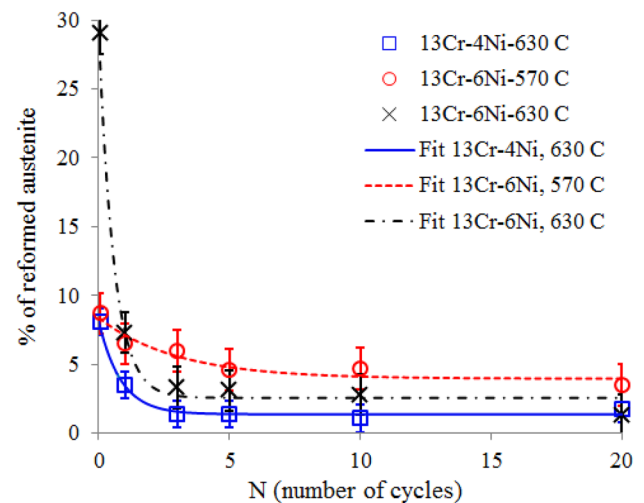


Fig. 4 Volume of reformed austenite versus number of cycles, $\Delta\varepsilon=2\%$, $R=-1$

tempered at 630 °C, corresponding to the maximum reformed austenite content at 8%. Two samples of the 13%Cr-6%Ni steel have been investigated. The first one with reformed austenite content equivalent to the reference (9%, tempered at 570 °C) and the other with maximum austenite content (29%, tempered at 630 °C).

The mechanical stability of reformed austenite was then documented using 2% strain controlled LCF tests for the three chosen conditions. The evolution of austenite content with the number of cycles, i.e. the transformation rate of reformed austenite can be seen on Fig. 4. The initial 8% reformed austenite found in the 13%Cr-4%Ni steel transforms almost entirely to martensite after 5 cycles, leaving a remaining amount of 1.5%, a value near the detection limit of X-ray scattering techniques. In the 13%Cr-6%Ni steel, the initial 9% austenite was found to transform at a much slower rate and remained at a volume fraction of about 4% after 5 cycles. Finally, the 13%Cr-6%Ni steel sample with maximum austenite amount transforms massively upon the first cycle and reaches an asymptote at around 2% after only 3 cycles.

The fraction of untransformed austenite has been deduced from the three curves shown on Fig. 4 by normalizing the data by the initial austenite percentages. The results, given in Fig. 5 show clearly that the 13%Cr-6%Ni tempered at 570 °C really stands out as being the steel bearing the most stable austenite: it is the one transforming at the slowest rate and having the highest fraction of untransformed austenite after 20 cycles. The 13%Cr-6%Ni steel tempered at 630 °C and the reference steel 13%Cr-4%Ni tempered at 630 °C, have much less stable austenite.

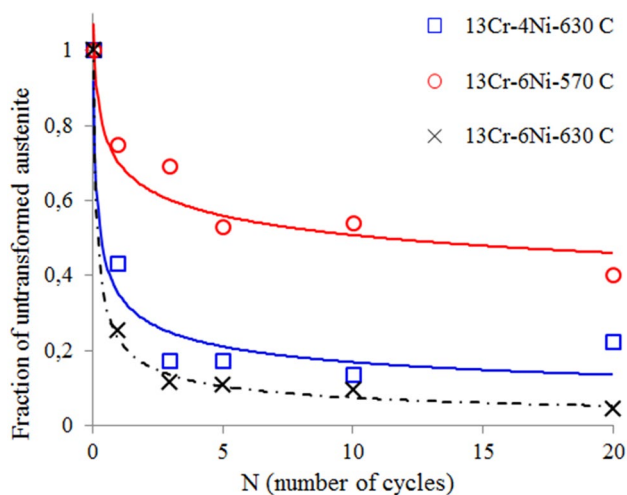


Fig. 5 Fraction of untransformed austenite versus number of cycles, $\Delta\varepsilon = 2\%$, $R = -1$

In order to quantify this transformation kinetic, an exponential regression analysis of the scaled curves has been run using the following relation:

$$F_{\gamma}(N) = V_{\gamma}(N)/V_o = ae^{(-bN)} + c \tag{1}$$

where $F_{\gamma}(N)$ is the remaining volume fraction of reformed austenite, N is the number of strain cycles, b represents the transformation rate (the smaller b the slower the austenite transformation), and c is the quantity of reformed austenite remaining after an infinite number of cycle. Finally, a is a scale factor, such that $a + c = 1$. From the analytical description of the experimental data, the rate of transformation per cycle can be calculated and constants determined as:

$$dF_{\gamma}(N)/dN = -abe^{(-bN)} \tag{2}$$

The normalized results are plotted in Fig. 6 and show that Eq. 2 correctly describes austenite behavior. Reformed austenite present in 13%Cr–6%Ni steel tempered at lower temperature transforms nine times slower than the one found in the same steel tempered at 630 °C and twice as slow as the 13%Cr–4%Ni steel tempered at about the same reformed austenite amount (8%).

Some hypotheses can be drawn from the results of Fig. 6:

- The high stability of the reformed austenite in 13%Cr–6%Ni tempered at 570 °C could be due to a significantly higher content in γ -stabilizers, such as Ni and Mn.
- The reformed austenite in 13%Cr–6%Ni tempered at 610 °C is the least stable of all, because its γ -stabilizers are diluted in a much higher volume fraction and ends up being in a lower concentration compared to the other steels.

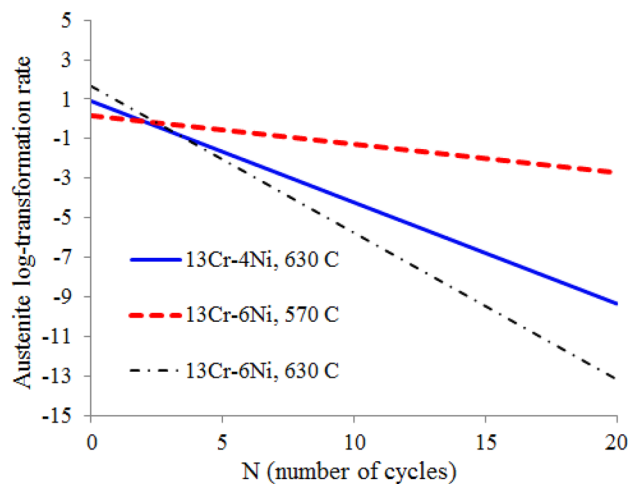


Fig. 6 Reformed austenite transformation rate versus number of cycles, $\Delta\varepsilon = 2\%$, $R = -1$

These hypotheses will be quantitatively tested in the following sections: experimentally by EDX, and by thermodynamic calculations using CalPhaD predictions along with the Thermo-Calc Software.

4 Microstructure of reformed austenite

The morphology of the reformed austenite in un-etched electropolished samples was studied by SEM observations. In Fig. 7, martensite is seen in dark grey, contrasting with light grey lamellar austenite and the bright carbides spots; the same contrast among phases is observed for all conditions. Reformed austenite phase has mostly been found to be lamellar with dimensions given in Table 4. The thinnest austenite lamellae are found in the 13%Cr–6%Ni steel tempered at 570 °C, followed by the 13%Cr–4%Ni tempered at 630 °C even if both steels have the same austenite percentage. The lamellae of the 13%Cr–6%Ni tempered at 570 °C are actually very small with an average thickness of 65 nm. This is twice thinner than the lamellae of 13%Cr–4%Ni steel tempered at 630 °C and 3.3 times thinner than in the same steel tempered at 630 °C.

In order to characterize the partition of elements into reverted austenite during intercritical tempering, TEM analyses were realized on samples for each tempering conditions. Some TEM images of the 13%Cr–6%Ni material tempered at 570 °C are presented in Fig. 8. Observations realized in bright field conditions in Fig. 8a, b show a lamella rich in austenite phase having a thickness of about 55 nm and formed between two larger martensite laths of thickness between 200 and 350 nm or more.

Selected Area Electron Diffraction (SAED) in Fig. 8d validated the austenitic composition of lamella in the

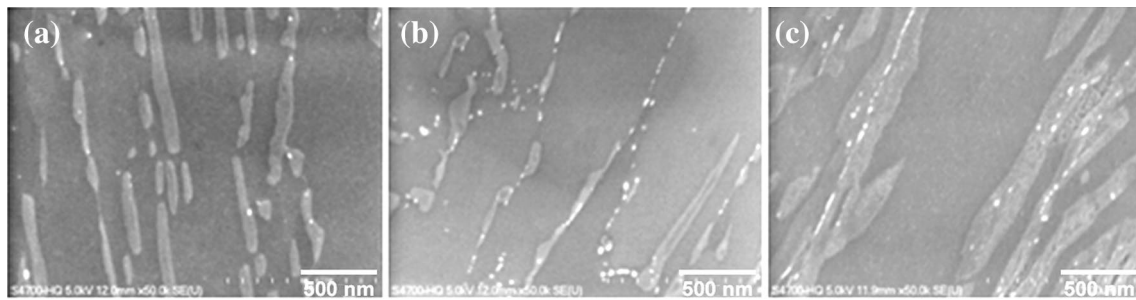


Fig. 7 Reformed austenite morphology: **a** 13Cr-4Ni, 630 °C, 8% γ , **b** 13Cr-6Ni, 570 °C, 9% γ , **c** 13Cr-6Ni, 630 °C, 29% γ

Table 4 Austenite lamellae width (measured on 100 lamellas)

| Steels | Austenite lamellae width (nm) and standard deviation |
|--------------------------------|--|
| 13Cr-4Ni, 630 °C, 8% γ | 132 ± 36 |
| 13Cr-6Ni, 570 °C, 9% γ | 65 ± 28 |
| 13Cr-6Ni, 630 °C, 29% γ | 215 ± 69 |

martensite matrix. Moreover, an austenitic lamella was clearly visible in the dark field image (Fig. 8c) obtained using the (111) diffraction spot of γ phase from the corresponding SAED.

Some small carbide precipitates, having diameter around 10 nm, seem also dispersed in the analyzed region in both martensitic and austenitic phases and along the lath boundaries. Other studies show the coexistence of nanometric carbides with austenitic phase, in particular at the boundaries with martensitic laths [26, 27]. In the present study, further microscopic investigations would be necessary to characterize them and define their composition and structure in relationship with γ and α phases.

Although the rather small lamellae width (typically below 100 nm) and the sample thickness can compromise precise composition measurements by EDX, as unwanted contributions from the surrounding martensitic matrix can be measured, some measurements have been run

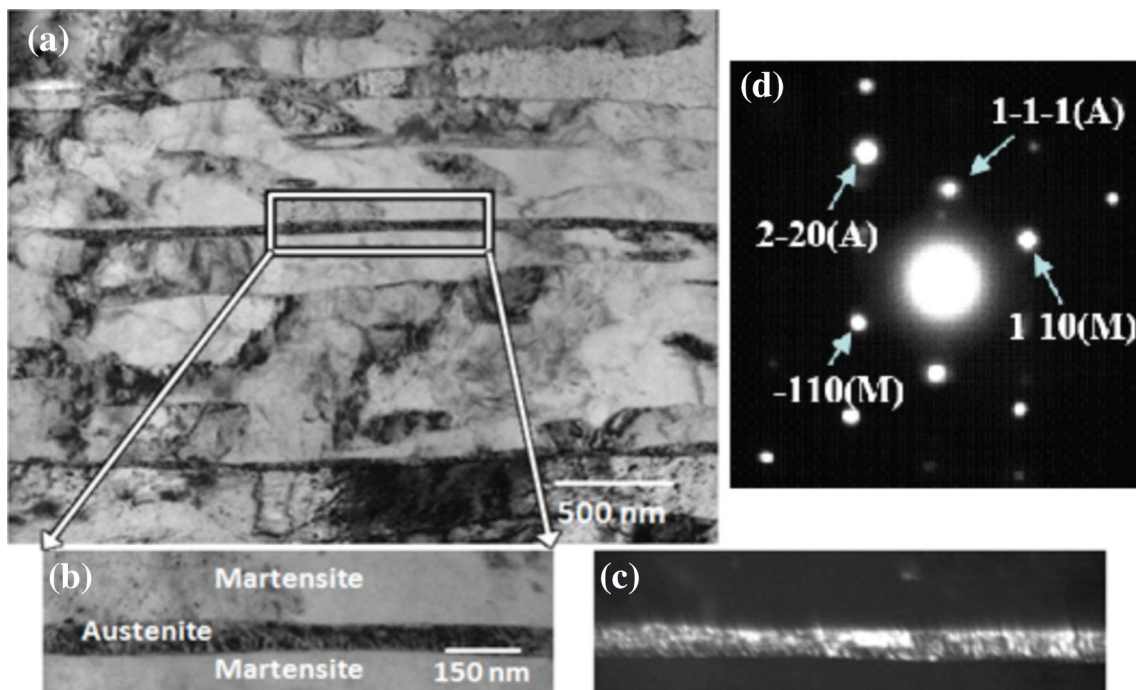


Fig. 8 TEM images of sample 13%Cr-6%Ni tempered at 570 °C for 1 h containing 9% of reformed austenite. **a** bright field image, **b** magnification of the region delimited by the rectangle in **a**. **c** dark

field of **b** centered on an austenite diffraction spot, and **d** corresponding SAD patterns from **b**

and reported below for consistency. These results will be compared later to thermodynamic theory prediction using Thermo-Calc Software.

4.1 Phase composition measurements

To document the relative chemical stability in the three studied microstructures, the partitions of Ni and Mn elements were measured in both phases. EDX maps were performed on different regions of the samples. Examples of these maps are given in Fig. 9 for the main austenite stabilizers (Ni and Mn) in order to show austenite enrichment. Segregation is more evident for nickel and particularly significant in the samples tempered at the higher temperature. The small size of austenite in the condition tempered at 570 °C may explain the weak contrast in composition as some of the matrix will interfere during the composition mapping. Moreover, in the latter segregation regions (the ones formed at 630 °C) some very bright regions can be seen in the contrast images in the first row of images in Fig. 9a, c. As it will be discussed later, this electronic contrast is due to the presence of dislocation tangles in fresh martensite laths, showing that segregation of nickel may

not be enough to stabilize the all the reverted austenite. This will be confirmed later by estimating M_s temperatures using various models.

Table 5 reports the average compositions of both phases measured in three spots for the three conditions. The 13%Cr–6%Ni steel treated at 570 °C concentrates less γ -stabilizer elements in the austenite than when tempered at 630 °C: this should thus logically predict that austenite formed at lower temperatures will be less stable than the one formed at higher temperatures. This is in clear contradiction with the LCF results that shows very that 13%Cr–6%Ni steel tempered at 570 °C has the most stable austenite of all. These contradictory results will now be put in contrast to some thermodynamic calculation done with Thermo-Calc.

4.2 Phase composition prediction using Thermo-Calc

Thermodynamic simulations were made using Thermo-Calc and the TCFE7 database. The results are presented in Table 6. Thermo-Calc modeling predicts that the austenite stabilizer fraction in austenite decreases when the

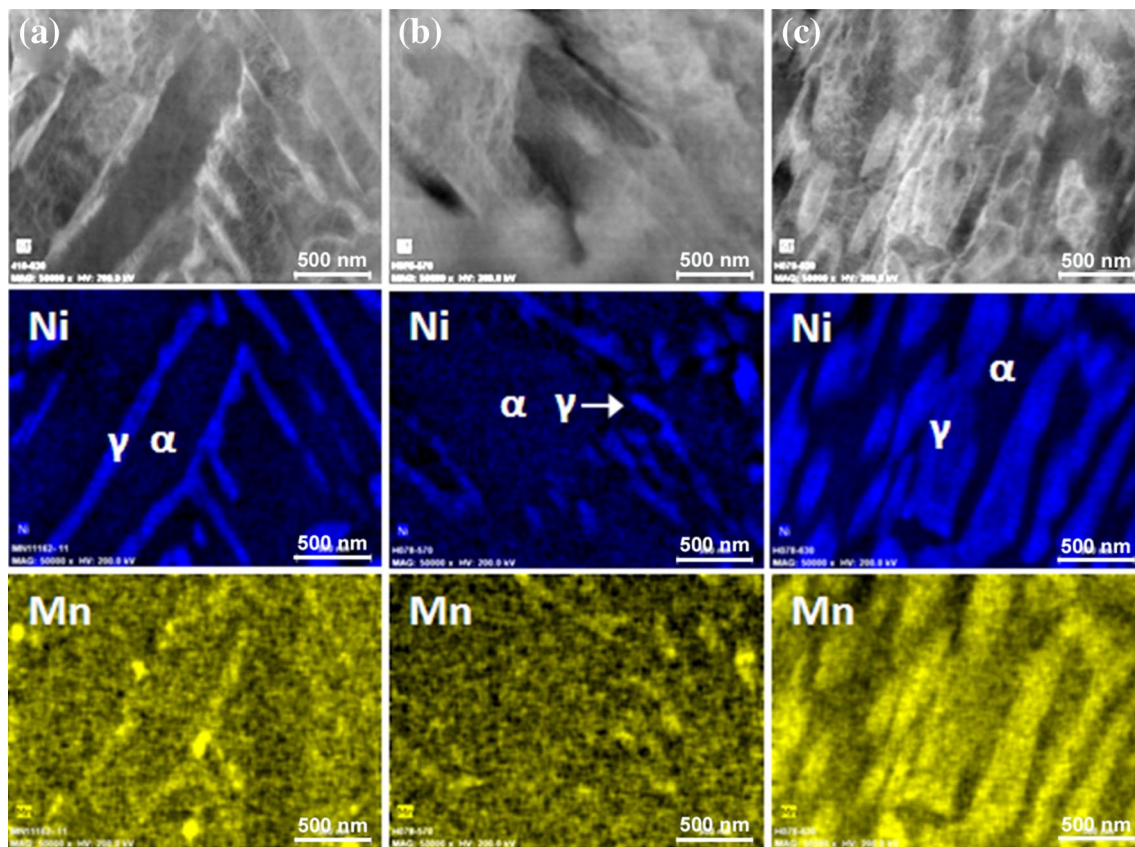


Fig. 9 STEM images and composition maps for Ni and Mn partitioning in the three materials: **a** 13%Cr–4%Ni, 630 °C, 8% γ **b** 13%Cr–6%Ni, 570 °C, 9% γ , **c** 13%Cr–6%Ni, 630 °C, and 29% γ

Table 5 EDX-STEM measured chemical composition of martensite (α) and reformed austenite (γ)

| Steels | % γ (XRD) | %Mn | | %Ni | | %Cr | |
|-------------------------|------------------|----------|----------|----------|----------|----------|----------|
| | | γ | α | γ | α | γ | α |
| 13%Cr–4%Ni (630 °C/1 h) | 8 | 0.33 | 0.05 | 8.34 | 3.63 | 13.7 | 12.6 |
| 13%Cr–6%Ni (570 °C/1 h) | 9 | 1.43 | 1.09 | 7.36 | 5.39 | 12.9 | 13.4 |
| 13%Cr–6%Ni (630 °C/1 h) | 29 | 1.74 | 0.37 | 8.51 | 3.53 | 12.9 | 12.6 |

Measurements errors are within 2%

Table 6 Volume fraction and chemical composition of martensite (α) and reformed austenite (γ) at equilibrium predicted by Thermo-Calc and TCFE7 iron and steels database (wt%)

| Steels | % γ | %Mn | | %Ni | | %C | |
|---------------------|------------|----------|----------|----------|----------|----------------------|----------------------|
| | | γ | α | γ | α | γ | α |
| 13%Cr–4%Ni (630 °C) | 18 | 1.22 | 0.20 | 10.4 | 3.35 | 6.6×10^{-4} | 2.8×10^{-5} |
| 13%Cr–6%Ni (570 °C) | 25 | 4.35 | 0.48 | 14.7 | 3.41 | 3×10^{-3} | 1.2×10^{-5} |
| 13%Cr–6%Ni (630 °C) | 53 | 2.32 | 0.46 | 9.11 | 2.95 | 1.7×10^{-3} | 7.1×10^{-5} |

tempering temperature increases, supporting the idea that less γ -stabilizer elements partition in the austenite phase. However, it predicts that a higher fraction of Mn and Ni will be found in the austenite at thermodynamic equilibrium and that about twice more reformed austenite content should be formed, compared to the measured data, suggesting that thermodynamic equilibrium has not been reached after 1 h tempering.

Such a discrepancy is far beyond the error due to approximations involved in CalPhaD extrapolation method and must be explained. Since at these high temperatures substitutional elements are extremely mobile even on significant distances, one can consider the system to be in ortho-equilibrium conditions, which means that the solute content of the austenite is roughly constant over the whole reversion process and the austenite composition is equal to the equilibrium solute content (as estimated by Thermo-Calc Software calculations). Assuming ortho-equilibrium conditions, and that TCFE7 Calphad database makes adequate predictions, a composition close to the equilibrium should be measured in all sample conditions and any discrepancies in term of composition between the measured and calculated values can only be attributed to measurement artefacts. A composition close to Thermo-Calc prediction is actually only measured in the sample where lamellae are, by far, the thickest. In the two other samples, lamella thicknesses are small and the contribution from the matrix reduces the measured Ni and Mn enrichment on EDX spectra. On the other hand, it is most likely that after only 1 h of heat treatment the thermodynamic volume fraction may have not been reached yet, explaining why the experimental volume fraction of austenite are significantly different from the estimated equilibrium values predicted by Thermo-Calc. This is in fact confirmed by results reported in other studies

on 13%Cr–4%Ni alloys of very similar compositions where reformed austenite were found to be as high as 27% after a 20 h temper [6, 28, 29].

In the case of the 13%Cr–6%Ni steel tempered 1 h at 570 °C, the measured compositions are significantly different from predictions with a measured percentage of Ni half of the calculated one. The size of austenite particles is significantly small in this condition (65 nm) and the X-ray interaction zone relatively large compared to lamella dimension, even for a small STEM spot size. Then, these measurements are likely averaging the austenite lamellae and the surrounding matrix reducing the reported value. This resulted in measuring lower solute contents in austenite than actual. This result is also consistent with the fact that 13%Cr–6%Ni steel exhibits at the same time the smaller lamella widths and the most dramatic difference in composition measurements compared with thermodynamic predictions, whereas agreement is not perfect but still rather good for both steels tempered at higher temperatures.

5 Estimating M_s as a stability indicator

5.1 Prediction from “non-adaptive regression”

From the compositions estimated with Thermo-Calc, it is also possible to estimate reverted austenite M_s using various methods. Simple linear regression methods are often applied, but one should realize that regression models are limited to the relative narrow range of alloy compositions used to obtain them. Lo and *al.* [30] provide four multiple regression formulas proposed for different authors that are in theory able to predict M_s for high chromium austenitic stainless steels. They are as follows:

$$M_s(^{\circ}C) = 546 - 12.1Cr\% - 7.5Mo\% - 17.7Ni\% - 423N\%$$

$$M_s(^{\circ}C) = 545 - 330C\% + 2Al\% + 7Co\% - 14Cr\% - 13Cu\% - 23Mn\% - 5Mo\% - 4Nb\% - 13Ni\% - 7Si\% + 3Ti\% + 4V\%$$

$$M_s(^{\circ}C) = A_{C3} - 199.8(C\% + 1.4N\%) - 17.9Ni\% - 21.7Mn\% - 6.8Cr\% - 45.0Si\% - 55.9Mo\% - 1.9(C\% + 1.4N\%)(Mo\% + Cr\% + Mn\%) - 14.4(Ni\% + Mn\%)(Cr\% + Mo\% + Al\% + Si\%)^{1/2} - 137$$

$$M_s(^{\circ}C) = 1037.2 - 302.3C\% + 8.6Co\% - 8.9Cr\% - 11.3Cu\% - 30.6Mn\% + 2.4Mo\% - 16.6Nb\% - 14.5Ni\% + 7.4W\%$$

and they are due to Andrews [31], Ishida [32], Dai and *al.* [33], and Capdevila and *al.* [34], respectively. The results are given on Table 7, for the three compositions predicted in the thermodynamic conditions. Except for Capdevila and *al.* [34] equation, all others predict very low M_s temperatures and cannot explain the presence of fresh martensite among the enriched lamellae (Fig. 9). Moreover, they cannot explain the poor stability of reformed austenite to LCF observed in the 13%Cr–4%Ni and 13%Cr–6%Ni tempered at 630 °C. On the other hand, M_s values significantly above ambient temperature predicted by Capdevila and *al.* [34] for the 13%Cr–6%Ni tempered 1 h at 570 °C and 630 °C well describe the above mentioned experimental observations. For example, the M_s value obtained for the 13%Cr–6%Ni tempered 1 h at 570 °C is relatively close to ambient temperature, this is consistent with the relatively high LCF stability for this condition.

Moreover, the significantly higher M_s values obtained for the conditions tempered at 630 °C (about 160 °C higher) predict the TEM observation that indicates that part of the reverted austenite formed during intercritical tempering at 630 °C was not retained at ambient temperature. However, the Capdevila and *al.* equation fails at predicting the relatively higher stability of the 13%Cr–4%Ni tempered 1 h at 630 °C compared to the 13%Cr–6%Ni tempered in the same conditions as the former has a higher M_s value than the latter.

5.2 Prediction from thermodynamic theory

The phenomenological model proposed by Ghosh and Olson [22, 23] was also used to estimate M_s . The results

were added to Table 7 and they show the better ability at predicting the stability of the alloys. The Ghosh and Olson model accounts for the micrograph evidences suggesting the presence of fresh martensite among the austenite dispersion enriched in Mn and Ni (Fig. 9) and the stability of the reformed austenite dispersion during low-cycle fatigue testing. In particular, the results were able to explain the slightly higher stability of the 13%Cr–4%Ni tempered at 630 °C for 1 h compared to the 13%Cr–6%Ni for the same tempering condition.

According to Ghosh and Olson model, the main cause for austenite stabilization is the segregation of the austenite-former elements during intercritical tempering. Other effects, such as the size and shape of the austenite dispersions or the hardness of the surrounding matrix could play a role on the austenite stability. However, these effects seems to play a secondary role since the physical based model by Ghosh and Olson models was able to correctly predict the LCF results for the three considered materials without considering these effects. Further development should consider these effects and will be the object of further experimental and modeling works.

Interestingly, the reason why Capdevila and *al.* [34] relation for M_s gave values close to the one obtained using physics theory and Thermo-Calc modeling as embedded into Ghosh and Olson models [22, 23] is likely due to the fact that it has been derived from a non-linear, data adaptive, neural network model using machine learning techniques. This kind of approach provides excellent opportunities to develop more statistically robust predictive tools from empirical results.

Table 7 Reverted austenite M_s using Thermo-Calc results with empirical models and Ghosh and Olson procedure

| Steels | Andrews | Ishida et al. | Dai et al. | Capdevila et al. | Ghosh and Olson |
|-----------------------------------|---------|---------------|------------|------------------|-----------------|
| 13%Cr–4%Ni (630 °C), 8% γ | –56 | –55 | –24 | 172 | 188 |
| 13%Cr–6%Ni (570 °C), 9% γ | –129 | –179 | –175 | 2 | 10 |
| 13%Cr–6%Ni (630 °C), 29% γ | –37 | –70 | 7 | 148 | 172 |

6 Conclusions

The purpose of this paper was to study the possibility of improving the mechanical stability under fatigue loading of the austenite contained in 13%Cr–4%Ni by increasing the amount of two austenite stabilizers, Ni and Mn. The microstructure of reformed austenite was investigated as a function of the tempering temperature for 1 h treatments and material composition for two compositions (13%Cr–4%Ni and 13%Cr–6%Ni alloys). The mechanical stability of reformed austenite was studied using 2% strain low-cycle fatigue tests at room temperature for one tempering condition for the 13%Cr–4%Ni and two conditions for the 13%Cr–6%Ni steel. The main conclusions from these experiments are:

- Increasing the amount of Ni from 4.62 mass% to 6.24 mass and Mn from 0.39 to 1.46 mass% leads to a larger temperature range between A_{C1} and A_{C3} , allowing an increase in reformed austenite content for a given tempering temperature. This allows similar amounts of austenite to be obtained while tempering in the intercritical range at lower temperatures.
- The maximum austenite volume fraction was achieved at the same temperature (630 °C) but the maximum volume was tripled, reaching up to 29% of austenite at room temperature.
- The sample tempered for 1 h at 570 °C has the lowest rate of transformation under low cycle fatigue tests revealing a reformed austenite with high stability.
- The higher stability achieved at a lower tempering temperature can be explained by a higher concentration of austenite stabilizers in a moderate volume fraction of reverted austenite, and, maybe, by a thinner reformed austenite lamellae.
- The M_s temperatures of the reformed austenite for the three mechanically tested steels were calculated using empirical and thermodynamic models. The physical model by Ghosh and Olson was the only method able to predict the respective stability of the steels under LCF.
- The calculation of reformed austenite M_s temperatures by Ghosh and Olson and Capdevilla and al. models showed that lower values are obtained at lower tempering temperatures. This explains the differences in LCF transformation kinetics observed experimentally when the steels were tempered at the lower temperature of 570 °C.
- When the maximum percentage of austenite was targeted (at 630 °C), the reformed austenite M_s temperatures were higher than room temperature, revealing that part of the reverted austenite obtained at the tem-

pering temperature transforms into fresh martensite under cooling (even if this tempering temperature generated the maximum reverted austenite).

- Some TEM observations support the fact that partial transformation takes place upon cooling after intercritical annealing at 630 °C.

The main conclusion and practical consequence of the present work is that optimal austenite mechanical stability can be achieved by tempering in the low temperature region of the intercritical phase field. This would yield larger austenite stabilizers concentrations in reverted austenite and minimize the size of the reformed austenite lamellae. Combining those two properties in the dispersed reformed austenite will be beneficial for resisting quenching and repetitive mechanical loading, providing better performances in usage.

Acknowledgements The authors wish to thank Alexandre Lapointe, Étienne Dallaire, René Dubois, Manon Provencher and René Veillette for their help in experimental tasks.

Data availability The data required to reproduce these findings cannot be shared at this time due to technical or time limitations/as the data also forms part of an ongoing study.

Compliance with ethical standards

Conflict of interest The authors declare that they have no conflict of interest.

References

1. Bilmes PD, Solari M, Llorente CL (2001) Characteristics and effects of austenite resulting from tempering of 13Cr–NiMo martensitic steel weld metals. *Mater Charact* 46:285–296
2. Gooch TG (1995) Heat treatment of welded 13%Cr–4%Ni martensitic stainless steels for sour service. *Weld J* 74:213–223
3. Song YY, Ping DH, Yin FX, Li XY, Li YY (2010) Microstructural evolution and low temperature impact toughness of a Fe–13%Cr–4%Ni–Mo martensitic stainless steel. *Mater Sci Eng A* 527:614–618
4. Lippold JC, Kotecki DJ (2005) *Welding metallurgy and weldability of stainless steels*. Wiley
5. Marshall AW, Farrar JCM (2001) *Soudage et techniques connexes*. 55:3–30
6. Amrei MM, Monajati H, Thibault D, Verreman Y, Bocher P (2015) Effects of various post-weld heat treatments on austenite and carbide formation in a 13Cr4Ni steel multipass weld. *Metallogr Microstruct Anal*. <https://doi.org/10.1007/s13632-015-0251-z>
7. Kimura M, Miyata Y, Toyooka T, Kitahaba Y (2001) Effect of retained austenite on corrosion performance for modified 13%Cr steel pipe. *Corrosion* 57:433–439
8. Song YY, Li XY, Ping DH, Rong L, Li YY (2010) Variation of the reversed austenite amount with the tempering temperature in a Fe–13%Cr–4%Ni–Mo martensitic stainless steel. *Mater Sci Forum* 650:193–198

9. Haynes AG (1999) Some factors governing the metallurgy and weldability of 13%Cr and newer Cr–Ni martensitic stainless steels. In: Supermartensitic stainless steels 99 conference proceedings, pp 25–32
10. Nakada N, Tsuchiyama T, Takaki S, Miyano N (2011) Temperature dependence of austenite nucleation behavior from lath martensite. *Iron Steel Inst Jpn* 51:299–304
11. Shin HC, Ha TK, Park WJ, Chang YW (2003) Deformation-induced martensitic transformation under various deformation modes. *Key Eng Mater* 233–236:667–672
12. Sugimoto K, Fiji D, Yoshikawa N (2010) Fatigue strength of newly developed high-strength low alloy TRIP-aided steels with good hardenability. *Procedia Eng* 2010(2):359–362
13. Benedetti M, Fontanari V, Barozzi M, Gabellone D, Tedesco MM, Plano S (2017) Low and high-cycle fatigue properties of an ultrahigh-strength TRIP bainitic steel. *Fatigue Fract Eng Mater Struct* 40:1459–1471
14. Robichaud P (2007) Stabilité de l'austénite résiduelle de l'acier inoxydable 415 soumis à la fatigue oligocyclique, Mémoire de maîtrise en génie mécanique, École de technologie supérieure, Montréal, Canada
15. Thibault D, Bocher P, Thomas M, Lanteigne J, Hovington P, Robichaud P (2011) Reformed austenite transformation during fatigue crack propagation of 13%Cr–4%Ni stainless steel. *Mater Sci Eng A* 528:6519–6526
16. Song YY, Li XY, Rong LJ, Li YY (2011) The influence of tempering temperature on the reversed austenite formation and tensile properties in Fe–13%Cr–4%Ni–Mo low carbon martensite stainless steels. *Mater Sci Eng A* 528:4075–4079
17. Haidemenopoulos GN, Grujicic M, Olson GB, Cohen M (1995) Thermodynamics-based alloy design criteria for austenite stabilization and transformation toughening in the Fe–Ni–Co system. *J Alloys Compd* 220:142–147
18. Totten GE, Howes MAH (1997) *Steel heat treatment handbook*. CRC Press, p 2
19. Jahn A, Kovalev A, Weiß A, Scheller PR (2011) Influence of manganese and nickel on the α' martensite transformation temperatures of high alloyed Cr–Mn–Ni Steels. *Steel Res Int* 82:1108–1112
20. Andersson JO, Helander T, Höglund L, Shi PF, Sundman B (2002) Thermo-Calc & DICTRA, computational tools for materials science. *Comput Tools Mater Sci* 26:273–312
21. Thermo-Calc Software TCFE, version 7. Accessed 15 May
22. Ghosh G, Olson GB (1994) Kinetics of F.C.C. \rightarrow B.C.C. heterogeneous martensitic nucleation—I. The critical driving force for athermal nucleation. *Acta Metall Mater* 42:3361–3370
23. Ghosh G, Olson GB (1994) Kinetics of F.c.c. \rightarrow b.c.c. heterogeneous martensitic nucleation—II. Thermal activation. *Acta Metall Mater* 42:3371–3379
24. Grujicic M, Olson GB, Owen WS (1985) Mobility of martensitic interfaces. *Metall Trans A* 16:1713–1722
25. Iwabuchi Y (2003) Factors affecting on mechanical properties of soft martensitic stainless steel castings. *JSME Int J* 46:441–446
26. Song YY, Li XY, Rong LJ, Ping DH, Yin FX, Li YY (2010) Formation of the reversed austenite during intercritical tempering in a Fe–13%Cr–4%Ni–Mo martensitic stainless steel. *Mater Lett* 64:1411–1414
27. Zhang S, Wang P, Li D, Li Y (2015) Investigation of the evolution of retained austenite in Fe–13%Cr–4%Ni martensitic stainless steel during intercritical tempering. *Mater Des* 84:385–394
28. Tenni B (2018) Étude expérimentale de l'effet du contenu inclusionnaire sur les propriétés mécaniques de résilience et de fatigue-propagation au seuil de soudures en acier 410 NiMo, M.Sc. thesis, École Polytechnique de Montréal
29. Fréchette G (2018) Étude du comportement au fluage de l'alliage 13Cr-4Ni en vue de simuler la redistribution des contraintes résiduelles lors du traitement thermique post-soudage. M.Sc. thesis, École de technologie supérieure
30. Lo KH, Shek CH, Lai JKL (2009) Recent developments in stainless steels. *Mater Sci Eng A* 65:39–104
31. Andrews KW (1965) Empirical formulae for the calculation of some transformation temperatures. *J Iron Steel Inst* 203:721–727
32. Ishida K (1995) Calculation of the effect of alloying elements on the M_s temperature in steels. *J Alloys Compd* 220:126–131
33. Dai QX, Cheng XN, Zha YT (2004) Design of martensite transformation temperature by calculation for austenitic steels. *Mater Charact* 52:349–354
34. Capdevila C, De Andrés CG (2002) "Determination of M_s temperature in steels: a Bayesian neural network model. *ISIJ Int* 42:894–902

Publisher's Note Springer Nature remains neutral with regard to jurisdictional claims in published maps and institutional affiliations.